46th AIAA Aerospace Sciences Meeting and Exhibit
7 - 10 January 2008, Reno, Nevada

AIAA 2008-778

46th AIAA Aerospace Sciences Meeting and Exhibit,January 7–10, 2008, Reno, NV

On the Geometric Conservation Law for High-order Discontinuous Galerkin Discretizations on Dynamically Deforming Meshes

Dimitri J. Mavriplis * and Cristian R. Nastase †

Department of Mechanical Engineering, University of Wyoming, Laramie, Wyoming 82071-3295

An approach for constructing high-order Discontinuous Galerkin schemes which preserve discrete conservation in the presence of arbitrary mesh motion, and thus obey the GCL, is derived. The approach is formulated for the most general case where only the coordinates defining the mesh elements are known at discrete locations in time, and results in the prescription of higher-order quadrature rules for certain terms in the governing equations in arbitrary Lagrangian Eulerian (ALE) form. For BDF1 temporal discretizations, the approach is exactly equivalent to a space-time formulation, while providing a natural extension to more complex discretizations such as BDF2. The method is shown to preserve the temporal accuracy of the underlying time-stepping scheme, for BDF1 and BDF2 schemes, for high-order spatial discretizations of the flow equations and mesh motion definition ranging up to fifth order accurate. Future work will investigate extensions of this approach to higher-order temporal schemes such as implicit Runge-Kutta schemes.

I. Introduction

Recently, there has been a growing interest in higher-order spatial discretization methods, due to the potential these methods offer for delivering high accuracy at reasonable cost. Discontinuous Galerkin methods in particular have enjoyed considerable success, partly due to the reliance of these methods on proven techniques in computational fluid dynamics, such as the use of approximate Riemann solvers, the ability to be formulated with a compact stencil, and the good scalability properties displayed on massively parallel computers.[1–4]

While much work has been performed with DG methods for steady-state or time-dependent problems on static meshes, relatively few investigations have looked at the formulation of DG methods on dynamically deforming meshes. The use of dynamically deforming meshes is important for many engineering applications with relative body motion, such as aeroelasticity. In order to use DG methods on moving meshes, the discretization must first be cast in Arbitrary Lagrangian Eulerian (ALE) form. This leads to the appearance of additional terms based on the velocities of the various grid entities such as vertices, faces and cells. An important consideration for unsteady moving mesh problems is whether these formulations preserve discrete conservation exactly. The statement of discrete conservation is embodied in the Geometric Conservation Law (GCL), which simply states that a uniform flow, which is an exact solution of any consistent discretization, should be preserved exactly in the presence of arbitrary mesh motion.

While much work has been devoted to studying the GCL and developing GCL compliant schemes for lower-order finite-volume schemes,[5–10] relatively little work has been done concerning the GCL for higher-order DG-type discretizations. At first the problem seems daunting, since not only the mesh coordinates vary in time, but the cell shape (curvature) time variations may also need to be taken into account, and all the basis and test functions vary in time as well. However, the use of iso-parametric mappings and elements, which is a standard approach in finite element formulations, enables the mesh deformation issues to be largely encapsulated in the form of a time-dependent iso-parametric mapping, thus retaining the use of constant basis functions in the iso-parametric space.[11]

Previous work on ALE formulations[11,12] for DG methods have most often assumed that the mesh velocities are known analytically, which is generally not the case for most engineering problems. Rather, the mesh point positions are known at the discrete locations in time (*i.e.* the time steps), since these are usually calculated by time-integrating a set of partial-differential equations which govern the mesh motion. Furthermore, previous work has mostly considered explicit time-integration strategies, and the effect of higher-order temporal discretizations has not been studied.

*Professor, AIAA Associate Fellow; email: mavripl@uwyo.edu.
†Postdoctoral Research Associate, AIAA Member; email: nastase@uwyo.edu.

Copyright © 2008 by Dimitri J. Mavriplis and Cristian R. Nastase. Published by the American Institute of Aeronautics and Astronautics, Inc., with permission.

In this work, we consider the formulation of DG-based discretization schemes which are GCL compliant, given only the knowledge of the mesh point positions at discrete time levels, in the context of low-order as well as higher-order time-integration schemes. The formulation is derived for the Euler equations in two-dimensions, although extensions to the Navier-Stokes equations and three-dimensions appear to be straight-forward.

II. Governing Equations

In an Eulerian framework, the conservative form of the compressible Euler equations describing the conservation of mass, momentum and total energy are given in vectorial form as:

$$\frac{\partial \mathbf{U}(\mathbf{x},t)}{\partial t} + \nabla \cdot \mathbf{F}(\mathbf{U}) = 0 \tag{1}$$

subject to appropriate boundary and initial conditions within a domain Ω. Explicitly, the state vector $\mathbf{U}$ of the conservative variables and the Cartesian components of the inviscid flux $\mathbf{F} = (\mathbf{F}^x, \mathbf{F}^y, \mathbf{F}^z)$ are:

$$\mathbf{U} = \begin{pmatrix} \rho \\ \rho u \\ \rho v \\ \rho w \\ E_t \end{pmatrix}, \quad \mathbf{F}^x = \begin{pmatrix} \rho u \\ \rho u^2 + p \\ \rho uv \\ \rho uw \\ u(E_t + p) \end{pmatrix}, \quad \mathbf{F}^y = \begin{pmatrix} \rho v \\ \rho uv \\ \rho v^2 + p \\ \rho vw \\ v(E_t + p) \end{pmatrix}, \quad \mathbf{F}^z = \begin{pmatrix} \rho w \\ \rho uw \\ \rho vw \\ \rho w^2 + p \\ w(E_t + p) \end{pmatrix}, \tag{2}$$

where ρ is the fluid density, (u,v,w) are the fluid velocity Cartesian components, p is the pressure and E_t is the total energy. For an ideal gas, the equation of state relates the pressure to total energy by:

$$p = (\gamma - 1)\left[E_t - \frac{1}{2}\rho(u^2 + v^2 + w^2)\right] \tag{3}$$

where $\gamma = 1.4$ is the ratio of specific heats.

III. Discontinuous Galerkin Discretization

III.A. Semi-discrete Formulation

The computational domain $\Omega(t)$ is partitioned into an ensemble of non-overlapping elements and within each element the solution is approximated by a truncated polynomial expansion

$$\mathbf{U}(\mathbf{x},t) \approx \mathbf{U}_p(\mathbf{x},t) = \sum_{j=1}^{M} \mathbf{u}_j(t)\phi_j(\mathbf{x}) \tag{4}$$

where M is the number of modes defining the truncation level. The semi-discrete formulation (*i.e.* continuous in time) employs a local discontinuous Galerkin formulation[1,13–15] in spatial variables within each element Ω_k. The weak formulation for Eq. (1) is obtained by minimizing the residual with respect to the expansion function in an integral sense:

$$\int_{\Omega_k(t)} \phi_i \left[\frac{\partial \mathbf{U}_p(\mathbf{x},t)}{\partial t} + \nabla \cdot (\mathbf{F}(\mathbf{U}_p)\right]_k d\Omega_k(t) = 0 \tag{5}$$

Because the domain of integration varies with time for moving mesh problems, the time derivative in the first term of the integrand is taken outside the integral using the following differential identity:

$$\frac{\partial}{\partial t}\int_{\Omega_k(t)} \phi_i \mathbf{U}_p d\Omega_k(t) = \int_{\Omega_k(t)} \frac{\partial \phi_i \mathbf{U}_p}{\partial t} d\Omega_k(t) + \int_{\Omega_k(t)} \nabla \cdot \phi_i \mathbf{U}_p \mathbf{U}_g d\Omega_k(t) \tag{6}$$

where $\mathbf{U}_g$ denotes the velocity of the domain of integration, which corresponds to the mesh velocity for a moving mesh when the integral is broken down into individual mesh element contributions.
Expanding the right hand side we obtain:

$$\frac{\partial}{\partial t}\int_{\Omega_k(t)} \phi_i \mathbf{U}_p d\Omega_k(t) = \int_{\Omega_k(t)} \phi_i \frac{\partial \mathbf{U}_p}{\partial t} + \mathbf{U}_p \frac{\partial \phi_i}{\partial t} d\Omega_k(t) + \int_{\Omega_k(t)} \phi_i \nabla \cdot \mathbf{U}_p \mathbf{U}_g + \mathbf{U}_p \mathbf{U}_g \nabla \cdot \phi_i d\Omega_k(t) \tag{7}$$

We next observe that the substantial derivative of the basis functions with respect to the grid motion must vanish, due to the fact that the basis functions move with the grid velocity. This is simply another expression of the fact that the basis functions are invariant in isoparametric space. Mathematically, this corresponds to the statement:

$$\frac{D\phi_i}{Dt} = 0 \tag{8}$$

where $\frac{D}{Dt}$ denotes the substantial derivative with respect to the grid motion, or alternatively:

$$\frac{\partial \phi_i}{\partial t} + \mathbf{U}_g \nabla \cdot \phi_i = 0 \tag{9}$$

resulting in the cancelation of the second and fourth terms in Eq. (7) as:

$$\int_{\Omega_k(t)} \mathbf{U}_p \frac{\partial \phi_i}{\partial t} d\Omega_k(t) + \mathbf{U}_p \mathbf{U}_g \nabla \cdot \phi_i d\Omega_k(t) = 0 \tag{10}$$

Therefore, Eq. (7) can be written as

$$\int_{\Omega_k(t)} \phi_i \frac{\partial \mathbf{U}_p}{\partial t} d\Omega_k(t) = \frac{\partial}{\partial t} \int_{\Omega_k(t)} \phi_i \mathbf{U}_p d\Omega_k(t) - \int_{\Omega_k(t)} \phi_i \nabla \cdot \mathbf{U}_p \mathbf{U}_g d\Omega_k(t) \tag{11}$$

Upon substituting this identity into equation (5), and integrating by parts, the weak statement of the problem becomes:

$$\frac{\partial}{\partial t} \int_{\Omega_k} \phi_i \mathbf{U}_p \, d\Omega_k - \int_{\Omega_k} \nabla \phi_i \cdot (\mathbf{F}(\mathbf{U}_p) - \mathbf{U}_g \mathbf{U}_p) \, d\Omega_k + \int_{\partial \Omega_k} \phi_i (\mathbf{F}^*(\mathbf{U}_p) - \mathbf{U}_g \mathbf{U}_p) \cdot \mathbf{n} \, d(\partial \Omega_k) = 0 \tag{12}$$

The local discontinuous Galerkin approach makes use of element-based basis functions, which results in solution approximations which are local, discontinuous, and doubled valued on each elemental interface. Monotone numerical fluxes are used to resolve the discontinuity, providing the means of communication between adjacent elements and specification of the boundary conditions. The numerical flux, $\mathbf{F}^*(\mathbf{U}_p) \cdot \mathbf{n}$, is obtained as a solution of a local one-dimensional Riemann problem and depends on the internal interface state, $\mathbf{U}_p^-$, the adjacent element interface state, $\mathbf{U}_p^+$ and the orientation as defined by the unit normal vector, $\mathbf{n}$, of the interface. An approximate Riemann solver is used to compute the flux at inter-element boundaries. Current implementations include the flux difference splitting schemes of Rusanov,[16] Roe,[17] HLL[18] and HLLC.[19–21]

The discrete form of the local discontinuous Galerkin formulation is defined by the particular choice of the set of basis functions, $\{\phi_i, i = 1 \ldots M\}$. The basis set is defined on an iso-parametric master element $\widehat{\Omega}(\xi_j, j = 1 \ldots 3)$ spanning between $\{-1 < \xi_j < 1\}$. We seek a set of hierarchical basis functions in order to simplify our subsequent spectral multigrid implementation. The basis set contains *vertex*, *edge* and *bubble* functions[22,23] based on Jacobi polynomials of variable weights. Since the basis set is defined in the master element, a coordinate transformation, $\mathbf{x}_p = \mathbf{x}_p(\xi_1, \xi_2, \xi_3)$, is required to compute the derivatives and the integrals in physical space $\Omega_k(x, y, z)$. For iso-parametric elements, the basis functions are expressed as functions of ξ_1, ξ_2 and ξ_3, and the coordinate transformation, and its Jacobian are given by:

$$\mathbf{x}_p = \sum_{j=1}^{M} \widehat{\mathbf{x}}_j \phi_j(\xi_1, \xi_2, \xi_3), \qquad J_k(\xi_1, \xi_2, \xi_3) = \left| \frac{\partial(x, y, z)}{\partial(\xi_1, \xi_2, \xi_3)} \right| \tag{13}$$

In the simple case of straight-sided or -faced elements the mapping is linear and its Jacobian, J_k, and its metrics are constant within each element, and can be evaluated just by using the element vertex coordinates. In the case of elements with curved faces, additional information must be provided in order to determine the coordinate expansion coefficients, $\widehat{\mathbf{x}}_j$. For the general case (*i.e.* curved elements), using Eq. (13), the solution expansion and the weak statement within each isoparametric element, $\widehat{\Omega}_k$, becomes:

$$\mathbf{U}_p(\xi, \eta, t) = \sum_{j=1}^{M} \widehat{\mathbf{u}}_j(t) \phi_j(\xi_1, \xi_2, \xi_3) \tag{14}$$

$$\frac{\partial}{\partial t} \int_{\widehat{\Omega}_k} \phi_i \mathbf{U}_p \, |J_k| d\widehat{\Omega}_k - \int_{\widehat{\Omega}_k} \nabla \phi_i \cdot (\mathbf{F}(\mathbf{U}_p) - \mathbf{U}_g \mathbf{U}_p) J_k^{-1} |J_k| d\widehat{\Omega}_k + \int_{\partial \widehat{\Omega}_k} \phi_i (\mathbf{F}^*(\mathbf{U}_p) - \mathbf{U}_g \mathbf{U}_p) \cdot \mathbf{n} \, |J_k| d(\partial \widehat{\Omega}_k) = 0 \tag{15}$$

One advantage of writing the discrete equations as integrals over the isoparametric elements $\widehat{\Omega}_k$ in the place of the physical mesh elements Ω_k, is that the iso-parametric elements are constant in time, and the dynamic motion of the mesh is now represented in the time-dependence of the Jacobian of the mapping $J_k(t)$. The semi-discrete form given by equation (15) can be written symbolically as:

$$\frac{d(\mathbf{M}\mathbf{U}_p)}{dt} + \mathbf{R}(\mathbf{U}_p, \mathbf{U}_g) = 0 \tag{16}$$

where $\mathbf{M}$ and $\mathbf{R}(\mathbf{U}_p, \mathbf{U}_g)$ represent the volume-integrated mass matrix and the non-linear residual associated with the master element $\widehat{\Omega}_k$, respectively. This system of ordinary differential equations is solved in modal space and the integrals are evaluated by economical Gaussian quadrature rules,[22,24,25] which requires a projection of the solution values to the quadrature points used in the numerical integration. In order to preserve $p+1$ accuracy order of the numerical approximation, the element integral uses quadrature rules which are exact for polynomial degree $2p$ within the master element, while the boundary integral uses quadrature rules which are exact for polynomial degree $2p+1$.[26] For boundary elements with curved edges or faces, the Jacobians must be evaluated at the integration quadrature points, whereas for interior elements with straight edges or faces, these are constant and need only be evaluated once for each element.

IV. Geometric Conservation Law

In order to guarantee discrete conservation in ALE form, the geometric conservation law must be satisfied. Briefly stated, the GCL corresponds to the statement that no disturbances should be introduced by any arbitrary mesh motion for a uniform flow. GCL formulations for finite-volume discretizations in ALE form have been studied extensively,[5–9] mostly for low-order temporal discretizations. More recently, GCL formulations for finite-volume schemes with high-order temporal discretizations have also been derived.[10,27] On the other hand, relatively little work on GCL formulations for high-order spatial discretizations has been performed. For discontinuous Galerkin discretizations, most previous work considering the GCL[11,12] has been based on the assumption of analytically defined grid velocities, and without regard for temporal accuracy concerns.

The more realistic situation is one where only the grid point positions are known at each discrete location in time, since these are most often obtained through the time-integration of a set of partial differential equations which are used to model the mesh motion, such as in the case of spring analogy or linear elasticity analogy mesh deformation strategies.[28–30] In this work, we consider the formulation of DG-based discretization schemes which are GCL compliant, given only the knowledge of the mesh point positions at discrete time levels, in the context of low-order as well as higher-order time-integration schemes.

IV.A. GCL Statement

The mathematical statement of the GCL is obtained by inserting a uniform flow field into equation (15), which after simplification becomes:

$$\frac{\partial}{\partial t}\int_{\widehat{\Omega}_k} \phi_i \, |J_k| d\widehat{\Omega}_k = -\int_{\widehat{\Omega}_k} \nabla\phi_i \cdot \mathbf{U}_g J_k^{-1} |J_k| d\widehat{\Omega}_k + \int_{\partial\widehat{\Omega}_k} \phi_i \mathbf{U}_g \cdot \mathbf{n} \, |J_k| d(\partial\widehat{\Omega}_k) \tag{17}$$

Equation (17) corresponds to a constraint on the grid velocities $\mathbf{U}_g$ which must be verified for each test function $\phi_i, i = 1,2,..,n$, and for the particular temporal discretization scheme chosen to advance the left-hand-side in time. There is not necessarily a one-to-one correspondence between the number of constraints (equations) and number of unknown grid velocity variables in Eq. (17), and it is therefore not evident how to impose this GCL condition.

IV.B. Space-Time Formulation

The most consistent approach for deriving fully conservative ALE formulations is by resorting to a space-time formulation. A fully conservative space-time discretization will automatically satisfy the GCL, and can be obtained simply by performing all required integrations on the space-time element exactly and consistently.

The space-time formulation begins by re-writing the governing equations (Eq. (1)) as:

$$\nabla_{\mathbf{xt}} \cdot \mathbf{G}(\mathbf{U}) = 0 \tag{18}$$

where $\mathbf{G}(\mathbf{U}) = [\mathbf{U}, \mathbf{F}(\mathbf{U})]^T$, and $\nabla_{\mathbf{xt}} = \left[\frac{\partial}{\partial t}, \frac{\partial}{\partial x_i}\right]^T$ denotes the space-time gradient operator. The weak statement for the governing equations is obtained by multiplying by a test function $\Phi(x_i,t)$ and integrating over space-time as:

$$\int_t^{t+\Delta t} \int_{\Omega_k} \Phi(x_i,t) \nabla_{\mathbf{xt}} \cdot \mathbf{G}(\mathbf{U}) d\Omega_k dt = 0 \tag{19}$$

Integrating by parts, yields:

$$-\int_t^{t+\Delta t} \int_{\Omega_k} \nabla_{\mathbf{xt}} \Phi(x_i,t) \cdot \mathbf{G}(\mathbf{U}) d\Omega_k dt + \int_t^{t+\Delta t} \int_{\partial\Omega_k} \Phi(x_i,t) \mathbf{G}(\mathbf{U}) \cdot \mathbf{n}\, d(\partial\Omega_k) dt = 0 \tag{20}$$

Next we must choose an appropriate form for the space-time basis functions. This is done by using a tensor product form in space and time as:

$$\Phi(x_i,t) = \phi(x_i)\psi(t) \tag{21}$$

where $\phi(x_i)$ represents the same basis functions previously used in the spatial DG formulation, and the choice $\psi(t) = 1$ is used for simplicity to reproduce a first-order temporal integration scheme (BDF1) at this preliminary stage. Substituting this form of the basis functions into Eq. (20), dividing through by the constant $\psi(t) = 1$, and reverting to the spatial formulation yields:

$$-\int_t^{t+\Delta t} \int_{\Omega_k} \frac{\partial \phi_i}{\partial t} \mathbf{U} + \nabla \phi_j \cdot \mathbf{F}(\mathbf{U}) d\Omega_k dt + \int_t^{t+\Delta t} \int_{\partial\Omega_k} \phi_i \left[\mathbf{U} \cdot \mathbf{n_t}\right] + \mathbf{F}(\mathbf{U}) \cdot \mathbf{n_x}\; d(\partial\Omega_k) dt = 0 \tag{22}$$

where n_t refers to the normal component in the time direction, and n_x refers to the normal component in the space direction. Invoking the isoparametric mapping, and re-writing these integrals in terms of their contributions from the various faces of the space-time element, it can be shown that the equations take on a more familiar form given by:

$$\begin{aligned} \int_{\widehat{\Omega}} \phi_i^{n+1} \mathbf{U}^{n+1} |J_k|^{n+1} d\widehat{\Omega}_k - \int_{\widehat{\Omega}(t)} \phi_i^n \mathbf{U}^n |J_k|^n d\widehat{\Omega}_k \quad &= \\ \int_t^{t+\Delta t} \int_{\widehat{\Omega}_k} \nabla \phi_i \cdot \left[\mathbf{F}(\mathbf{U}_p) - \mathbf{U}_p \mathbf{U}_g\right] J_k^{-1} |J_k| d\widehat{\Omega}_k dt \quad &- \quad \int_t^{t+\Delta t} \int_{\partial\widehat{\Omega}_k} \phi_i \left[\mathbf{F}^*(\mathbf{U}_p) - \mathbf{U}_p \mathbf{U}_g\right] \cdot \mathbf{n} |J_k| d(\partial\widehat{\Omega}_k) dt \end{aligned} \tag{23}$$

The next step is to expand the solution in terms of the basis functions in order to obtain a system of algebraic equations to be solved. Since we have chosen a constant variation in time within the space-time element (*i.e.* $\psi(t) = 1$), it should be evident that all the solution values on the right-hand side of the above equation are to be evaluated at the $n+1$ time step, which corresponds to the constant value in the time interval $[t^n, t^{n+1}]$. This formulation thus corresponds to a first-order backwards time-integration scheme (BDF1).

In order to complete the integration, we also need functional forms for the grid velocities $\mathbf{U_g}$. Since these terms arise from the integration on the inclined surfaces of the space-time element, their temporal and spatial variation must be determined by the shape of the space-time element, which is ultimately determined by the grid point locations in space and time constituting the element, as well as their functional form. If the grid point coordinates are given as a function of time only at the points $t = t^n$ and $t + \Delta t = t^{n+1}$, then the space-time element vertices must be joined by straight-line segments in the time direction, as shown in Figure (1), and the grid velocities must be constant in time. A spatial variation of the grid velocities is obtained by expanding the grid velocities in terms of the same basis functions used for the solution expansion:

$$\mathbf{U}_g = \sum_{i=1}^{M} \phi_i(x,y,z) \hat{u}_g \tag{24}$$

and the modal coefficients $\hat{u}_g$ are determined such that the grid velocities match the values calculated by differentiating the time-dependent grid-point coordinates at known locations in space. For example, if the grid vertex positions for a triangular mesh are known at individual time steps, as depicted in Figure 1, the grid velocities take on a linear variation in space (and are constant over each time step) and are given by:

$$\mathbf{U}_g = \sum_{i=1}^{3} \phi_i \frac{x_i(t+\Delta t) - x_i(t)}{\Delta t} \tag{25}$$

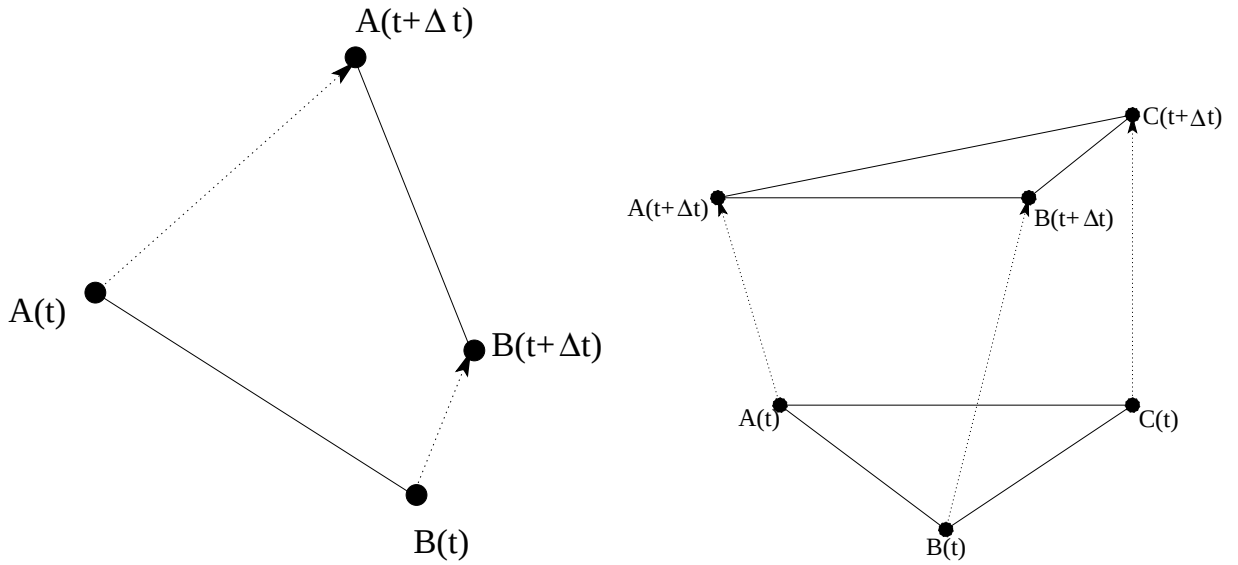

(a) Space-time element and area swept by moving edge

(b) Space-time element and volume swept by moving triangular element

Figure 1.

where x_i represents the coordinates of the three vertices of the triangle. For deforming curved elements, higher order variations of the grid velocities are required, but can be easily handled using this framework, noting that this requires the knowledge of additional element point positions as a function of time, in order to define the time-dependent element curvature. Note that the spatial and temporal variation of the grid velocities can be independent (higher or lower order) than that of the flow solution itself, and is determined solely by the formulation used to compute the mesh motion.

Once the solution and grid velocities are expanded in terms of the spatial basis functions, the integration of the right-hand side of Eq. (23) must be performed exactly using sufficiently high-order quadrature, in the usual manner for discontinuous Galerkin formulations. For the spatial integrals, the extra terms such as $\mathbf{U}_p\mathbf{U}_g$ due to the grid motion involve higher-order variations in space, resulting in the need to use appropriately higher accuracy quadrature rules. In the case of linear spatial variations for the grid velocities, the order of integration must be raised by 1, although this must be increased further for dynamically deforming *curved* elements.

Because the terms $J_k^{-1}|J_k|$ and $\mathbf{n}|J_k|$ in the volume and surface integrands, respectively, depend on the mesh coordinates, and thus vary (non-linearly) in time, the temporal integration will also require increased quadrature orders, *even though we have assumed constant solution values and grid velocities within the space-time element.* The appropriate quadrature rules in time are determined by examining the functional form of the temporal variation of these terms. When all the space-time integrals are evaluated exactly, a BDF1 DG scheme which automatically satisfies the GCL is obtained.

In order to verify that the GCL is indeed verified, a constant solution can be substituted into Eq. (23) in order to get obtain GCL condition:

$$\begin{aligned}\int_{\widehat{\Omega}} \phi_i^{n+1}|J_k|^{n+1}d\widehat{\Omega}_k - \int_{\widehat{\Omega}(t)} \phi_i^{n}|J_k|^{n}d\widehat{\Omega}_k \quad &= \\ -\int_t^{t+\Delta t}\int_{\widehat{\Omega}_k} \nabla\phi_i\cdot\mathbf{U}_g J_k^{-1}|J_k|d\widehat{\Omega}_k dt \quad &+ \quad \int_t^{t+\Delta t}\int_{\partial\widehat{\Omega}_k}\phi_i\mathbf{U}_g\cdot\mathbf{n}\,|J_k|d(\partial\widehat{\Omega}_k)dt\end{aligned} \tag{26}$$

which corresponds to the time-integrated form of Eq. (17). For first-order accurate $p = 0$ discretizations, where the spatial basis functions ϕ_i reduce to a single constant function on each element, the above equation reduces to:

$$\int_{\widehat{\Omega}(t+\Delta t)} |J_k|^{n+1}d\widehat{\Omega}_k - \int_{\widehat{\Omega}(t)} |J_k|^{n}d\widehat{\Omega}_k = \int_t^{t+\Delta t}\int_{\partial\widehat{\Omega}_k}\mathbf{U}_g\cdot\mathbf{n}\,|J_k|d(\partial\widehat{\Omega}_k)dt \tag{27}$$

which corresponds to the expression derived for finite-volume schemes in references.[10,27] Furthermore, the exact integration of the boundary terms on the right-hand-side of this equation requires a mid-point quadrature rule in two-dimensions, and a two-point quadrature rule in three dimensions. This corresponds to the formulation previously derived in references[7,10,27] for calculating the area swept by the control volume faces in time.

V. Higher-Order Temporal Integration

While the space-time formulation with constant basis functions in time provides an elegant approach for formulating a GCL compliant ALE scheme, it is only first-order accurate in time and thus is of limited practical use. The obvious extension of this approach to higher-order temporal schemes is to use higher order temporal basis functions $\psi = \psi(t)$ in the space-time formulation. Note that the space-time formulation described so far corresponds to a discontinuous Galerkin method in space and in time. Discontinuous Galerkin methods in time have been examined in the literature and have been shown to be equivalent to implicit Runge-Kutta (IRK) methods[31] under certain conditions. Thus, in order to implement a GCL compliant IRK scheme, the appropriate basis functions in time which correspond to the particular IRK scheme must be determined. This may be a non-trivial task for Diagonally Implicit Runge-Kutta (DIRK) schemes, which are currently the preferred approach for higher-order temporal schemes due to their lower computational expense.[32–34] Additionally, for second-order backwards-difference (BDF2) schemes, which are often used in computational engineering problems, there is no simple set of element-based basis functions which can be used, since the temporal stencil of a BDF2 scheme extends beyond the current time-element.

Traditionally, most time-integration schemes in computational fluid dynamics are derived using the method of lines, whereby the spatial terms are first discretized, and then the resulting system of coupled ordinary differential equations are integrated in time using a BDF, IRK, or other time-integration scheme. Thus, for example, a BDF1 scheme applied to the semi-discrete form of the governing equations given by Eq. (15) gives:

$$\begin{aligned} \frac{1}{\Delta t}\left[\int_{\widehat{\Omega}_k} \phi_i \mathbf{U}_p^{n+1} |J_k|^{n+1} d\widehat{\Omega}_k - \int_{\widehat{\Omega}_k} \phi_i \mathbf{U}_p^{n} |J_k|^{n} d\widehat{\Omega}_k\right] &= \\ \int_{\widehat{\Omega}_k} \nabla\phi_i \cdot (\mathbf{F}(\mathbf{U}_p^{n+1}) - \mathbf{U}_g^{n+1}\mathbf{U}_p^{n+1}) J_k^{-1} |J_k| d\widehat{\Omega}_k &- \int_{\partial\widehat{\Omega}_k} \phi_i (\mathbf{F}^*(\mathbf{U}_p^{n+1}) - \mathbf{U}_g^{n+1}\mathbf{U}_p^{n+1}) \cdot \mathbf{n} |J_k| d(\partial\widehat{\Omega}_k) \end{aligned} \tag{28}$$

where all the spatial terms on the right-hand side are evaluated at the latest time step $n+1$, as prescribed by the backwards-difference formula. The problem with this formulation is that the grid velocities are ill-defined at the location $n+1$ in time, since the grid point coordinates are given at these locations, but the velocities must be obtained by finite differencing the coordinates in time. Furthermore, the simple-minded approach of calculating the grid velocities at the required quadrature points as the differences of coordinates in time (divided by the time step) results in a non-conservative scheme which violates the GCL.

In order to determine a suitable formulation for the grid velocities, the GCL for the BDF1 discretization is written, either by substituting a uniform flow-field into Eq. (28), or by applying the BDF1 formula to the semi-discrete GCL statement given by Eq. (17), which yields:

$$\frac{1}{\Delta t}\left[\int_{\widehat{\Omega}_k} \phi_i |J_k|^{n+1} d\widehat{\Omega}_k - \int_{\widehat{\Omega}_k} \phi_i |J_k|^{n} d\widehat{\Omega}_k\right] = -\int_{\widehat{\Omega}_k} \nabla\phi_i \cdot \mathbf{U}_g^{n+1} J_k^{-1} |J_k| d\widehat{\Omega}_k + \int_{\partial\widehat{\Omega}_k} \phi_i \mathbf{U}_g^{n+1} \cdot \mathbf{n} |J_k| d(\partial\widehat{\Omega}_k) \tag{29}$$

Comparing this equation with the space-time formulation (*i.e.* Eq. (26)), which is known to automatically satisfy the GCL, it becomes evident that the right-hand-side integrals in the above equation must correspond to the mean value of the corresponding time integrals in Eq. (26), or specifically:

$$\int_{\widehat{\Omega}_k} \nabla\phi_i \cdot \mathbf{U}_g^{n+1} J_k^{-1} |J_k| d\widehat{\Omega}_k = \frac{1}{\Delta t}\int_{t^n}^{t^{n+1}} \int_{\widehat{\Omega}_k} \nabla\phi_i \cdot \mathbf{U}_g J_k^{-1} |J_k| d\widehat{\Omega}_k dt \tag{30}$$

and

$$\int_{\partial\widehat{\Omega}_k} \phi_i \mathbf{U}_g^{n+1} \cdot \mathbf{n} |J_k| d(\partial\widehat{\Omega}_k) = \frac{1}{\Delta t}\int_{t^n}^{t^{n+1}} \int_{\partial\widehat{\Omega}_k} \phi_i \mathbf{U}_g \cdot \mathbf{n} |J_k| d(\partial\widehat{\Omega}_k) dt \tag{31}$$

However, although these equations can be used to obtain values for the above spatial integrals of the grid velocities at the new time level, they do not yield values of the grid velocities themselves, and hence are of little use in evaluating the integrals in Eq. (28), since the integrands are multiplied by the solution vector in these integrals. Although the solution vector must be integrated in space, we recall that in both the BDF and space-time formulations, the solution vector is constant in time, within a given time step. Thus, an expression for the grid velocity integrands is obtained by reversing the order of the space-time integration, and dropping the spatial integral as:

$$\left[\nabla\phi_i \mathbf{U}_g J_k^{-1} |J_k|\right]^{n+1} = \frac{1}{\Delta t}\int_{t}^{t+\Delta t} \nabla\phi_i \cdot \mathbf{U}_g J_k^{-1} |J_k| dt \tag{32}$$

and

$$[\phi_i \mathbf{U}_g \cdot \mathbf{n}\,|J_k|]^{n+1} = \frac{1}{\Delta t}\int_t^{t+\Delta t} \phi_i \mathbf{U}_g \cdot \mathbf{n}\,|J_k| dt \tag{33}$$

where it is understood that the above equalities hold at any given constant location in isoparametric space, and thus at the quadrature points of the spatial integration. These expressions can therefore be used in evaluating the spatial integrals at the time level $n+1$ on the right-hand-side of Eq. (28). For example, the volume integral containing the grid speed term is evaluated as:

$$\int_{\widehat{\Omega}_k} \nabla\phi_i \cdot \mathbf{U}_g^{n+1}\mathbf{U}_p^{n+1} J_k^{-1}|J_k| d\widehat{\Omega}_k = \sum_{n=1}^{N_q} \omega_q \mathbf{U}_{p_q}^{n+1} \left[\nabla\phi_i \mathbf{U}_g J_k^{-1}|J_k|\right]_q^{n+1} \tag{34}$$

with a similar expression for the boundary term.

This construction is completely analogous to the space-time formulation given in the previous section, and thus is known to satisfy the GCL. Although this formulation is still only first-order accurate in time, it provides a framework for extending the approach to different time-integration schemes such as BDF2 and IRK schemes.
The BDF2 temporal discretization can be written as:

$$\frac{1}{\Delta t}\left[\frac{3}{2}\int_{\widehat{\Omega}_k} \phi_i \mathbf{U}_p^{n+1}|J_k|^{n+1} d\widehat{\Omega}_k - 2\int_{\widehat{\Omega}_k} \phi_i \mathbf{U}_p^{n}|J_k|^{n} d\widehat{\Omega}_k + \frac{1}{2}\int_{\widehat{\Omega}_k} \phi_i \mathbf{U}_p^{n-1}|J_k|^{n-1} d\widehat{\Omega}_k\right] = \tag{35}$$
$$\int_{\widehat{\Omega}_k} \nabla\phi_i \cdot (\mathbf{F}(\mathbf{U}_p^{n+1}) - \mathbf{U}_g^{n+1}\mathbf{U}_p^{n+1}) J_k^{-1}|J_k| d\widehat{\Omega}_k - \int_{\partial\widehat{\Omega}_k} \phi_i (\mathbf{F}^*(\mathbf{U}_p^{n+1}) - \mathbf{U}_g^{n+1}\mathbf{U}_p^{n+1}) \cdot \mathbf{n}\,|J_k| d(\partial\widehat{\Omega}_k)$$

which leads to the GCL statement:

$$\frac{1}{\Delta t}\left[\frac{3}{2}\int_{\widehat{\Omega}_k} \phi_i |J_k|^{n+1} d\widehat{\Omega}_k - 2\int_{\widehat{\Omega}_k} \phi_i |J_k|^{n} d\widehat{\Omega}_k + \frac{1}{2}\int_{\widehat{\Omega}_k} \phi_i |J_k|^{n-1} d\widehat{\Omega}_k\right] = -\int_{\widehat{\Omega}_k} \nabla\phi_i \cdot \mathbf{U}_g^{n+1} J_k^{-1}|J_k| d\widehat{\Omega}_k + \int_{\partial\widehat{\Omega}_k} \phi_i \mathbf{U}_g^{n+1} \cdot \mathbf{n}\,|J_k| d(\partial\widehat{\Omega}_k) \tag{36}$$

While this GCL statement cannot be directly related to the space-time formulation of Eq. (26), it can be seen to be the sum of two successive steps in the space-time formulation when written as:

$$-\int_{\widehat{\Omega}_k} \nabla\phi_i \cdot \mathbf{U}_g^{n+1} J_k^{-1}|J_k| d\widehat{\Omega}_k + \int_{\partial\widehat{\Omega}_k} \phi_i \mathbf{U}_g^{n+1} \cdot \mathbf{n}\,|J_k| d(\partial\widehat{\Omega}_k) = \tag{37}$$
$$\frac{3}{2\Delta t}\left[\int_{\widehat{\Omega}_k} \phi_i |J_k|^{n+1} d\widehat{\Omega}_k - \int_{\widehat{\Omega}_k} \phi_i |J_k|^{n} d\widehat{\Omega}_k\right] - \frac{1}{2\Delta t}\left[\int_{\widehat{\Omega}_k} \phi_i |J_k|^{n} d\widehat{\Omega}_k - \int_{\widehat{\Omega}_k} \phi_i |J_k|^{n-1} d\widehat{\Omega}_k\right]$$

and thus the expressions for the grid velocity terms at the spatial integration quadrature points become:

$$\left[\nabla\phi_i \mathbf{U}_g J_k^{-1}|J_k|\right]^{n+1} = \frac{3}{2\Delta t}\int_t^{t+\Delta t} \nabla\phi_i \cdot \mathbf{U}_g J_k^{-1}|J_k| dt - \frac{1}{2\Delta t}\int_{t-\Delta t}^{t} \nabla\phi_i \cdot \mathbf{U}_g J_k^{-1}|J_k| dt \tag{38}$$

and

$$[\phi_i \mathbf{U}_g \cdot \mathbf{n}\,|J_k|]^{n+1} = \frac{3}{2\Delta t}\int_t^{t+\Delta t} \phi_i \mathbf{U}_g \cdot \mathbf{n}\,|J_k| dt - \frac{1}{2\Delta t}\int_{t-\Delta t}^{t} \phi_i \mathbf{U}_g \cdot \mathbf{n}\,|J_k| dt \tag{39}$$

Using these expressions in the integrand of the spatial integrals on the right-hand-side of Eq. (35) results in a second-order accurate BDF temporal scheme which satisfies the GCL.

VI. Numerical Results

The validity of the aforementioned formulations for higher-order spatial discretizations has been verified numerically, using the deforming mesh where the grid motion is defined analytically as:

$$\mathbf{x}(t) = \mathbf{x}(t) + \mathbf{dx}(t) \tag{40}$$

where $\mathbf{x}$(t) is the grid coordinate vector and $\mathbf{dx}(t)$ is the displacement. For a two-dimensional space-time unity domain in $0 \le x, y, t \le 1$ the grid displacement is defined as

$$dx(t) = A_x \sin(f_n t)\sin(f_x x)\sin(f_y y) \tag{41}$$

$$dy(t) = A_y \sin(f_n t) \sin(f_x x) \sin(f_y y) \tag{42}$$

where, A_x and A_y are the amplitudes in $x-$ and $y-$directions and $f_{x,y}$ and f_n factors are used to define the number of periods in space and time, respectively. However, this motion is not general and must be modified in order to be applied to a domain and integration time of arbitrary size by introducing reference space and time lengths. Hence a more general way to define the grid motion is

$$dx(t) = A_x Lx\, dt/t_{max} \sin(f_n t) \sin(f_x x) \sin(f_y y) \tag{43}$$

$$dx(t) = A_y Ly\, dt/t_{max} \sin(f_n t) \sin(f_x x) \sin(f_y y) \tag{44}$$

where, dt represents the time step and $L_{x,y}$ and t_{max} denote the reference values for time and space respectively. The $f_{x,y}$ and f_n factors are defined as:

$$f_n = n_t \pi / t_{max} \tag{45}$$

$$f_x = n_x \pi / L_x \tag{46}$$

$$f_y = n_y \pi / L_y \tag{47}$$

where $n_{x,y}$ and n_t denote the number of half periods in space and time respectively. Figure (2) depicts the motion in the space-time unity domain ($L_x = L_y = t_{max} = 1$) and half time period ($n_t = 1$) for $n_x = n_y = 4$ and amplitude $A_x = A_y = 0.1$. Similarly, Figure (3) depicts the motion for $n_x = n_y = 8$ and amplitude $A_x = A_y = 0.05$.

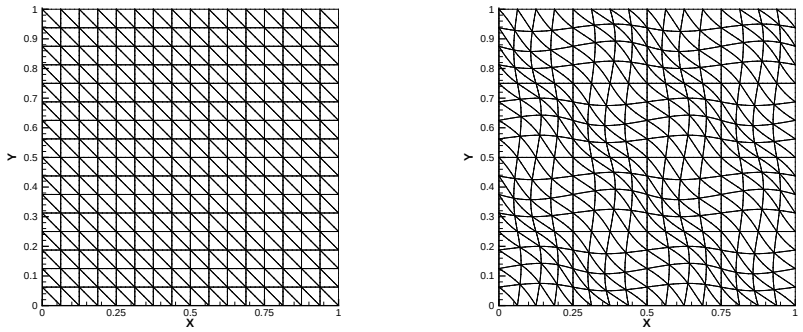

(a) t=0.0 (b) t=1/3

(c) t=2/3 (d) t=1.0

Figure 2. Moving mesh during half time period ,$n_t = 1$, using $n_x = n_y = 4$ half periods in space of amplitude $A_x = A_y = 0.1$.

This motion prescribes the position for the vertices and various points along each edge allowing for the use of high-order geometrical representation (*i.e.* curved elements). The polynomial order for the grid motion is chosen to be equal to the discretization order used for the field variables for all cases presented in this paper, although in principle these two orders can be prescribed independently.

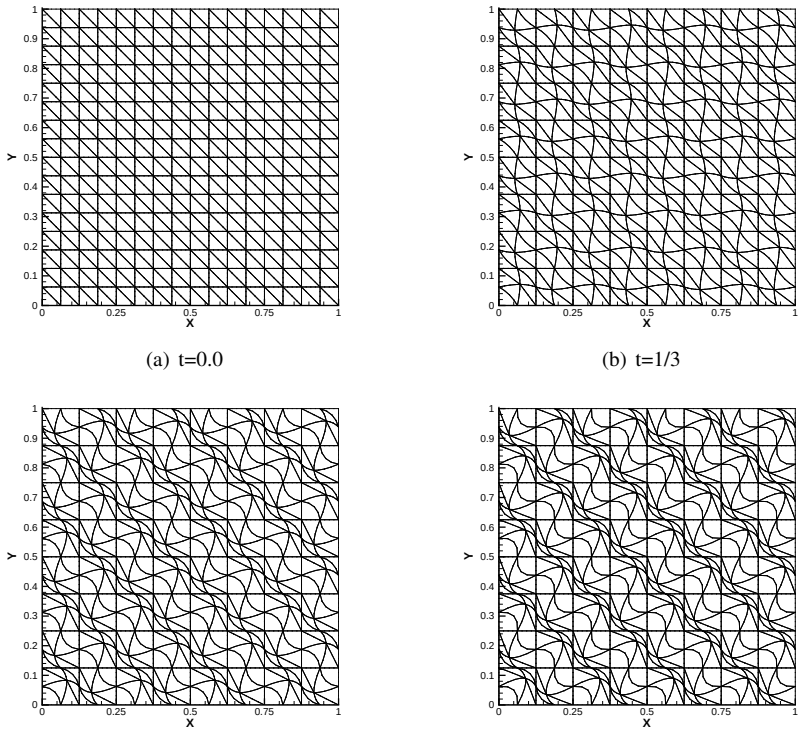

(a) t=0.0 (b) t=1/3

(c) t=2/3 (d) t=1.0

Figure 3. Moving mesh during half time period ,$n_t = 1$, using $n_x = n_y = 8$ half periods in space of amplitude $A_x = A_y = 0.05$.

VI.A. Free stream preservation

A uniform inviscid flow in the x-direction is considered on a square domain defined in $0 \leq x, y \leq 40$. The domain is partitioned in 512 unstructured cells and the mesh motion amplitude is set to $A_x = 1.0$ and $A_y = 1.0$. This produces a wave like motion, as depicted in Figure (3) for one period. Using the space-time formulation, as well as the BDF1 and BDF2 formulations with sufficiently high-order quadrature rules as described previously, the residual of the flow equation was verified to be of the order of machine precision at all time steps, for spatial orders ranging from $p = 0$ up to $p = 5$, thus verifying the discrete conservation property and GCL compliance of these different temporal discretizations.

VI.B. Temporal Accuracy Study: Convection of an isentropic vortex

A square domain defined in $0 \leq x, y \leq 40$ is considered for this case as well. The domain is partitioned in 2048 uniform triangular cells and the mesh motion amplitude is set to $A_x = 0.1$ and $A_y = 0.1$. A fifth-order accurate ($p = 4$) spatial discretization is used for all temporal schemes. The mean flow density, ρ_∞, velocity, u_∞ and v_∞, pressure, p_∞ and temperature T_∞ are taken as free stream values, which are set as $(\rho_\infty, u_\infty, v_\infty, p_\infty, T_\infty) = (1, 1, 0, 1, 1)$ in this test case. Free-stream boundary conditions are imposed on the top and bottom boundaries, At $t_0 = 0$, the flow is perturbed by an isentropic vortex $(\delta u, \delta v, \delta T)$ centered at (x_0, y_0) with the form:

$$\delta u = -\frac{\alpha}{2\pi}(y - y_0)e^{\phi(1-r^2)} \tag{48}$$

$$\delta v = \frac{\alpha}{2\pi}(x - x_0)e^{\phi(1-r^2)} \tag{49}$$

$$\delta T = -\frac{\alpha^2(\gamma - 1)}{16\phi\gamma\pi^2}e^{2\phi(1-r^2)} \tag{50}$$

where, ϕ and α are parameters which determine the strength of the vortex, $r = \sqrt{(x - x_0)^2 + (y - y_0)^2}$ is the distance to the vortex center, and $\gamma = 1.4$ is the ratio of specific heats of air. In this study, we set ϕ as unity and α as 4.0. Given the

perturbation functions shown in Eq. (48), (49) and (50), we can determine the other resulting conservative variables, assuming isentropic flow throughout the domain (i.e. $p/\rho^\gamma = 1$ and $T = p/\rho$ for a perfect gas):

$$\rho = T^{1/(\gamma-1)} = (T_\infty + \delta T)^{1/(\gamma-1)} = \left[1 - \frac{\alpha^2(\gamma-1)}{16\phi\gamma\pi^2} e^{2\phi(1-r^2)}\right]^{1/(\gamma-1)} \tag{51}$$

$$u = u_\infty + \delta u = 0.5 - \frac{\alpha}{2\pi}(y - y_0)e^{\phi(1-r^2)} \tag{52}$$

$$v = v_\infty + \delta v = 0 + \frac{\alpha}{2\pi}(x - x_0)e^{\phi(1-r^2)} \tag{53}$$

The initial vortex ($t = 0$) is placed at $(x_0, y_0) = (10, 10)$ as depicted in Figure (4) and is convected to $(x, y) = (30, 30)$ which corresponds to a final time $t_{max} = 28.3$. The obtained density contours at time $t = 3/4\,t_{max}$ obtained via the BDF1 and BDF2 schemes are shown in Figure (5(a)) and Figure (5(b)), respectively.

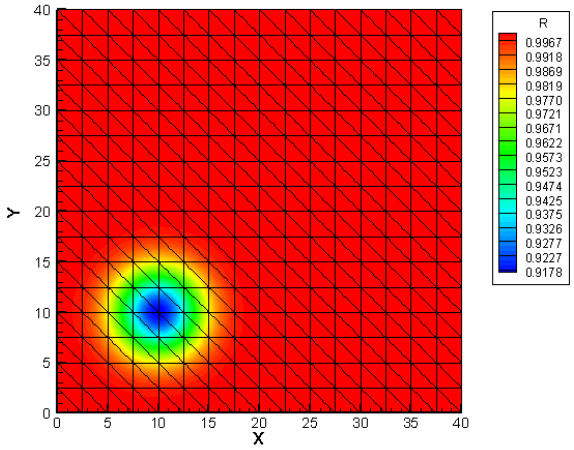

Figure 4. Initial density contours for $p = 4$ spatial discretization.

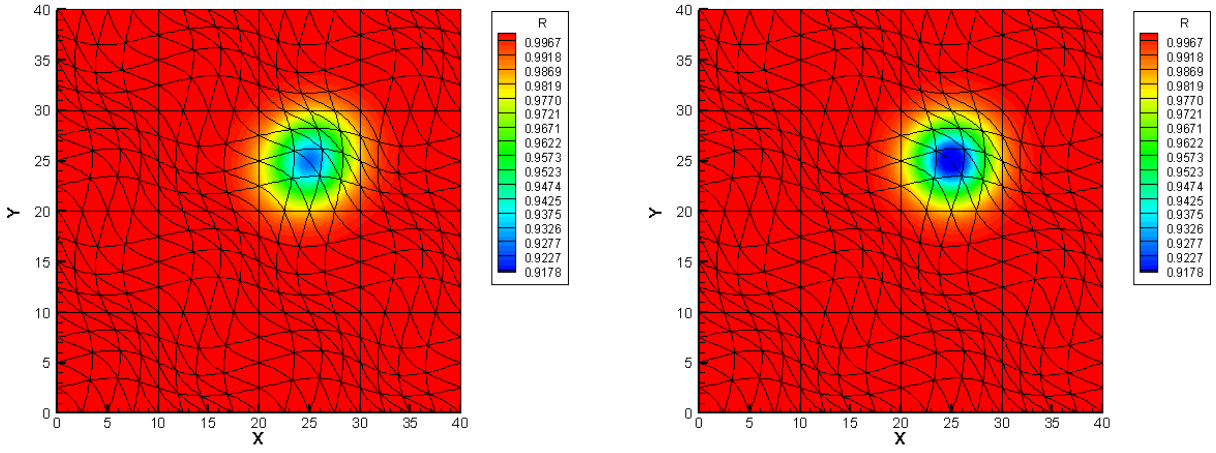

(a) BDF1 (b) BDF2

Figure 5. Density contours of the BDF1 and BDF2 schemes at time $t = 3/4\,t_{max}$ using a time-step of $\delta t = 0.25$ and $p = 4$ spatial discretization.

In order to assess the asymptotic behavior of the time-integration schemes, a temporal refinement study is carried out using a fixed spatial discretization ($p = 4$). The solution for each temporal scheme is obtained using a small time-step reference solution, in order to eliminate the effect of spatial error and to isolate the temporal error. The "exact" solution is obtained using a time-step of Δt = 0.01 for all time-integration schemes. Additionally, various

time-steps, $\Delta t = 0.0625$, 0.125, 0.25, 0.5, 1.0, 2.0 and 5.0, are used for all of the temporal schemes. The temporal error is obtained by computing the RMS difference of one conserved variable between the computed solution and the reference "exact" solution. The temporal accuracy results for the BDF1 and BDF2 schemes at $t = 10$ are illustrated in Figure (6), where the computed temporal error is plotted as a function of the time-step on a log-log plot. The first-order backwards-differencing scheme displays a slope of 0.87, while the second-order backwards-differencing scheme achieves a slope of 1.97. These results demonstrate that the chosen temporal discretization schemes achieve their design order of accuracy within the range of time steps of interest and for high-order spatial discretizations.

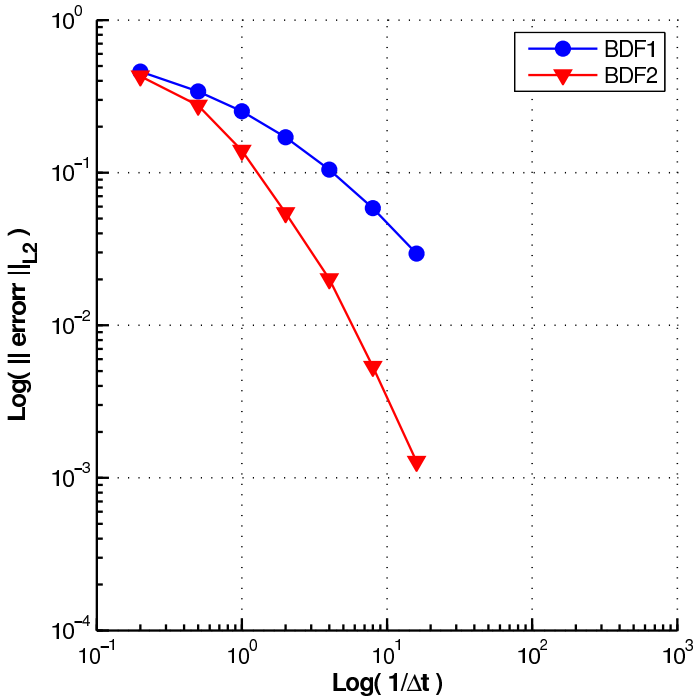

Figure 6. Temporal accuracy as a function of time-step size at $t = 10$.

VII. Conclusions and future work

An approach for constructing discretely conservative high-order Discontinuous Galerkin schemes which verify the GCL in the presence of dynamically deforming meshes has been derived in this work. The method allows for arbitrarily high-order for the spatial discretization of the flow equations as well as for the spatial order of the definition of the mesh motion. For BDF1 schemes, this approach is equivalent to a space-time formulation, but extends naturally to more complex temporal discretizations such as BDF2, while preserving the design temporal accuracy of underlying time-stepping scheme. The extension of this approach to alternate high-order temporal discretizations such as implicit Runge-Kutta schemes is currently under investigation. By formulating schemes as Discontinuous Galerkin schemes in time, the space-time formulation may be employed directly, using higher-order temporal basis functions. Alternatively, the present approach may be employed for each successive stage in an IRK scheme. Future work will investigate these two strategies and seek to demonstrate simultaneously high temporal and spatial accuracy with full discrete conservation in the presence of dynamically deforming meshes.

Acknowledgments

This work was partly supported by a grant from the Office of Naval Research under ONR grant number N00014-04-1-0602, as well as by NASA grant NNX07AC31A.

References

[1]Cockburn, B. and Shu, C.-W., "The Local Discontinuous Galerkin Method for Time-Dependent Convection-Diffusion Systems," *SIAM J. Numer. Anal.*, Vol. 35, No. 6, 1998, pp. 2440–2463.

[2]Cockburn, B., Karniadakis, G. E., and Shu, C. W., *Discontinuous Galerkin Methods: Theory, Computation and Applications*, Springer, 2000.

[3]Atkins, H. and Shu, C. W., "Quadrature-Free Implementation of Discontinuous Galerkin Method for Hyperbolic Equations," *AIAA Journal*, Vol. 36, No. 5, 1998, pp. 775–782.

[4]Nastase, C. and Mavriplis, D. J., "A Parallel hp-Multigrid Solver for Three-Dimensional Discontinuous Galerkin Discretizations of the Euler Equations," AIAA Paper 2007–0512, Jan 2007.

[5]Thomas, P. D. and Lombard, C. K., "Geometric Conservation Law and its Application to Flow Computations on Moving Grids," *AIAA Journal*, Vol. 17, No. 10, 1979, pp. 1030–1037.

[6]Zhang, H., Reggio, M., Trepanier, J. Y., and Camarero, R., "Discrete form of the GCL for moving meshes and its implementation in CFD schemes," *Computers and Fluids*, Vol. 22, 1993, pp. 9–23.

[7]Lesoinne, M. and Farhat, C., "Geometric conservation laws for flow problems with moving boundaries and deformable meshes, and their impact on aeroelastic computations," *Computer Methods in Applied Mechanics and Engineering*, Vol. 134, 1996, pp. 71–90.

[8]Guillard, H. and Farhat, C., "On the significance of the geometric conservation law for flow computations on moving meshes," *Computer Methods in Applied Mechanics and Engineering*, Vol. 190, 2000, pp. 1467–1482.

[9]Geuzaine, P., Grandmont, C., and Farhat, C., "Design and analysis of ALE schemes with provable second-order time-accuracy for inviscid and viscous flow simulations," *Journal of Computational Physics*, Vol. 191, 2003, pp. 206–227.

[10]Mavriplis, D. J. and Yang, Z., "Construction of the Discrete Geometric Conservation Law for High-Order Time Accurate Simulations on Dynamic Meshes," *Journal of Computational Physics*, Vol. 213, No. 2, 2006, pp. 557–573.

[11]Persson, P. and Peraire, J., "Discontinuous Galerkin Solution of the Navier-Stokes Equations on Deformable Domains," AIAA Paper 2007–0513, Jan. 2007.

[12]Lomtev, I., Kirby, R., and Karniadakis, G., "A Discontinuous Galerkin method in moving domains," In Proc. of Discontinuous Galerkin Methods: Theory, Computation and Applications, eds. Cockburn et al., Springer-Verlag, NY, 1999.

[13]Bassi, F. and Rebay, S., "High-Order Accurate Discontinuous Finite Element Solution of the 2D Euler Equations," *J. Comput. Phys.*, Vol. 138, 1997, pp. 251–285.

[14]Warburton, T. C., Lomtev, I., Du, Y., Sherwin, S. J., and Karniadakis, G. E., "Galerkin and Discontinuous Galerkin Spectral/*hp* Methods," *Comput. Methods Appl. Mech. Engrg.*, Vol. 175, 1999, pp. 343–359.

[15]Cockburn, B. and Shu, C.-W., "Runge-Kutta Discontinuous Galerkin Methods for Convection-Dominated Problems," *SIAM J. Sci. Comput.*, Vol. 16, No. 3, 2001, pp. 173–261.

[16]Davis, S. F., "Simplified Second-Order Godunov-Type Methods," *SIAM J. Sci. Statist. Comput.*, Vol. 9, No. 3, 1988, pp. 445–473.

[17]Roe, P. L., "Approximate Riemann Solvers, Parameter vectors, and Difference Schemes," *J. Comput. Phys.*, Vol. 43, 1981, pp. 357–372.

[18]Harten, A., Lax, P. D., and Van Leer, B., "On Upstream Differencing and Godunov-Type Schemes for Hyperbolic Conservation Laws," *SIAM Review*, Vol. 25, No. 1, 1983, pp. 35–61.

[19]Toro, F. E., *Riemann Solvers and Numerical Methods for Fluid Dynamics*, Applied Mechanics, Springer-Verlag, New York, NY, 1999.

[20]Batten, P., Clarke, N., Lambert, C., and Causon, D. M., "On the Choice of Wavespeeds for the HLLC Riemann Solver," *SIAM J. Sci. Comput.*, Vol. 18, No. 2, 1997, pp. 1553–1570.

[21]Batten, P., Leschiner, M. A., and Goldberg, U. C., "Average-State Jacobians and Implicit Methods for Compressible Viscous and Turbulent Flows," *J. Comput. Phys.*, Vol. 137, 1997, pp. 38–78.

[22]Solin, P., Segeth, P., and Zel, I., *High-Order Finite Element Methods*, Studies in Advanced Mathematics, Chapman and Hall, 2003.

[23]Szabo, B. and Babuska, I., *Finite Element Analysis*, John Wiley & Sons, Inc., New York, NY, 1991.

[24]Dunavant, D. A., "Highr Degree Efficient Symmetrical Gaussian Guadrature Rules for the Triangle," *Int. J. Numer. Meth. Engng.*, Vol. 21, 1985, pp. 1129–1148.

[25]Dunavant, D. A., "Economical Symmetrical Quadrature Rules for Complete Polynomials Over a Square Domain," *Int. J. Numer. Meth. Engng.*, Vol. 21, 1985, pp. 1777–1784.

[26]Cockburn, B., Hou, S., and Shu, C.-W., "The Runge-Kutta local projection discontinuous Galerkin finite element method for conservation laws IV: The multidimensional case," *Math. Comput.*, Vol. 54, No. 545, 1990.

[27]van Zuijlen, A. and Bijl, H., "High Order Time Integration For Fluid-Structure Interaction on Moving Meshes," AIAA 2005-5247, 2005.

[28]Degand, C. and Farhat, C., "A Three-Dimensional Torsional Spring Analogy Method for Unstructured Dynamic Meshes," *Computers and Structures*, Vol. 80, 2002, pp. 305–316.

[29]Baker, T. J., "Mesh Movement and Metamorphosis," *Engineering with Computers*, Vol. 18, No. 3, 2002, pp. 188–198.

[30]Yang, Z. and Mavriplis, D. J., "Unstructured Dynamic Meshes with Higher-order Time Integration Schemes for the Unsteady Navier-Stokes Equations," AIAA Paper 2005-1222, 2005.

[31]Estep, D., "A Posteriori Error Bounds and Global Error Control for Approximation of Ordinary Differential Equations," *SIAM Journal of Numerical Analysis*, Vol. 32, 1995, pp. 1–48.

[32]Bijl, H., Carpenter, M. H., and Vatsa, V. N., "Time Integration Schemes for the Unsteady Navier-Stokes Equations," AIAA 2001-2612, 2001.

[33]Jothiprasad, G., Mavriplis, D. J., and Caughey, D. A., "Higher-order time integration schemes for the unsteady Navier Stokes equations on unstructured meshes," *Journal of Computational Physics*, Vol. 191, 2003, pp. 542–566.

[34]Wang, L. and Mavriplis, D. J., "Implicit solution of the unsteady Euler equations for high-order accurate Discontinuous Galerkin discretizations," *Journal of Computational Physics*, Vol. 213, No. 2, 2007, pp. 557–573.